Supporting Information

Direct Proton-Coupled Electron Transfer between Interfacial Tyrosines in Ribonucleotide Reductase

Jiayun Zhong,[†] Clorice R. Reinhardt,[‡] and Sharon Hammes-Schiffer*[†]

†Department of Chemistry, Yale University, New Haven, Connecticut 06520, United States

‡Department of Molecular Biophysics and Biochemistry, Yale University, New Haven, Connecticut 06520, United States

* Corresponding author email: sharon.hammes-schiffer@yale.edu

Table of Contents

Methods

The system setup and classical molecular dynamics (MD) simulation protocols followed those used for our previous MD simulations of ribonucleotide reductase (RNR).[1] The quantum mechanical/molecular mechanical (QM/MM) free energy simulation protocols were adapted from our previous QM/MM free energy simulations of other collinear proton-coupled electron transfer (PCET) reactions in RNR.[2-3] These protocols are summarized here, with more details provided in the earlier work.

System Setup

All simulations started from the cryo-EM structure of the active $\alpha_2\beta_2$ complex of *E.coli* RNR (PDB ID: 6W4X).[4] We used H++ to add hydrogen atoms to the system at pH 7.[5] The protein complex was then immersed in a box of TIP3P water[6] neutralized with Na^+ ions. The salt concentration of the solution was then adjusted by adding Na^+ and Cl^- ions to be ~ 150 mM.

We used the ff14SB force field[7] for the classical MD and the molecular mechanical (MM) part of the QM/MM simulations. We also used the same force field parameters and partial charges for the diiron center in the β subunits, bound GDP and TTP molecules, and $Y356^{\bullet}$ or $Y731^{\bullet}$ as in our previous MD simulations of RNR.[1] In the prior work the MCPB.py utility[8] with AmberTools was used to derive partial charges of the diiron center, and the standard RESP[9] procedure was used to parameterize the tyrosyl radical. The electrostatics were treated with the particle mesh Ewald method,[10] and a cutoff distance of 10 Å was used for nonbonded interactions. We used the SHAKE algorithm[11] to constrain bond lengths involving hydrogen atoms and the SETTLE algorithm[12] to treat the triangulated TIP3P water[6] molecules. All MD simulations in this work used a time step of 1 fs. The MD in the NVT and NPT ensembles used a Langevin thermostat with a 2 ps^{-1} collision frequency, and the MD in the NPT ensemble used the Berendsen barostat.[11]

MD Equilibration

The energy minimization and MD steps for equilibration were the same as those used for our previous MD simulations of RNR.[1] The detailed energy minimization and MD procedures were as follows:

1. 5000 steps of minimization of the added solvent and ions using the steepest descent (SD) algorithm with harmonic restraints with force constants of 500 kcal/mol $Å^{-2}$ applied to the protein atoms.
2. 500 ps of NVT MD of the solvent and ions at 300 K using the same restraints on the protein atoms as the first minimization step.
3. 1 ns of NPT MD of the solvent and ions at 300 K and 1 atm pressure using the same restraints on the protein atoms as the first minimization step.
4. 2000 steps of minimization of the protein with SD and 3000 steps of minimization using the conjugate gradient (CG) algorithm with 100 kcal/mol $Å^{-2}$ harmonic restraints on the non-hydrogen atoms of the protein.
5. Minimization of the protein with 100, 50, and 10 kcal/mol $Å^{-2}$ harmonic restraints on the backbone atoms of the protein. Each minimization step entailed 2000 steps of minimization of with SD and 3000 steps of minimization using the CG algorithm.
6. 2500 steps of minimization of the protein with SD and 2500 steps with CG without any restraints.
7. 360 ps of NPT heating of the entire system from 0 K to 300 K at 1 atm. For each step, the temperature was increased 50 K over 10 ps followed by an additional 50 ps equilibration at each resulting temperature.
8. 20 ns of NPT MD equilibration of the system at 300 K and 1 atm.
9. 20 ns of NVT MD equilibration of the system at 300 K.

Classical MD Simulations

Eight independent MD trajectories with the radical on Y356 and another eight independent MD trajectories with the radical on Y731 were propagated. No other radicals were present in the system. Each of these independent trajectories was propagated for 100 ns in the NVT ensemble at 300 K. The average root-mean square deviation (RMSD) for the C_α atoms in the α/β subunits over all production trajectories with respect to the cryo-EM structure was 1.42 ± 0.15 Å for the system with $Y356^\bullet$ and 1.33 ± 0.19 Å for the system with $Y731^\bullet$ (Figure S2). The RMSD, number of hydrogen bonds, and Y356:O-Y731:O distance were computed using CPPTRAJ within AmberTools and further confirmed with MDAnalysis.[13-14]

QM/MM Free Energy Simulations

We used the QM/MM finite temperature string method with umbrella sampling to study the PCET reaction between Y356 and Y731. We propagated four independent strings: two strings for direct PCET with Y731 flipped out toward the α/β interface and two strings for the water-mediated PCET mechanism with Y731 either flipped out or stacked with Y730. These QM/MM free energy simulations were performed with the Amber/Q-Chem interface[15-17]. All nonbonded interactions were included without any cut-off for the QM/MM simulations. We used the ωB97X-D functional[18] and the 6-31+G** basis set[19-21] for the QM region and the AMBER ff14SB force field[7, 22-24] with the extensions described above for the MM region. The SCF convergence criteria for the DFT calculations was 10^{-6}. We have used the same functional and basis set for all our QM/MM free energy simulations of the PCET reactions in RNR,[2-3] and we showed that this level of theory is consistent with complete active space self-consistent field with second-order perturbative corrections (CASSCF+NEVPT2) calculations on related model systems for PCET between a tyrosine or a cysteine and a tyrosyl radical.

Each independent string was started from an MD equilibrated solvated protein system. To prepare for the QM/MM free energy simulations, all water molecules and ions beyond 5 Å of any protein residue or nucleotide were removed from the system unless they were within 18 Å of Y731:O. This produced a system containing around 60,000 atoms, which is tractable for QM/MM simulations. The QM region included the sidechains of Y356 and Y731 for all the strings, plus the bridging water for the water-mediated PCET string with flipped Y731, and plus the bridging water and the sidechain of Y730 for the water-mediated PCET string with stacked Y731 (Figure S1). The link atoms were placed at the QM and MM region boundaries, namely between C_β and C_γ of the two tyrosines, automatically by the Amber QM/MM interface.[16] The direct PCET strings, the water-mediated PCET string with flipped Y731, and the water-mediated PCET string with stacked Y731 contain 31, 34, and 50 atoms, respectively, in their QM regions including link atoms. Since there are no residues other than water within ~3.5 – 4.0 Å of Y356:O or Y731:O to impact the free energy landscapes, we did not include other amino acid residues in the QM region. Three reaction coordinates were used for the direct PCET strings, and six reaction coordinates were used for the water-mediated PCET strings, which involved double proton transfer (Figure S1).

An important consideration for QM/MM simulations is the size of the QM region, which has been shown to influence simulation results for some systems.[25] In previous work,[2] we computed

the free energy surfaces for PCET between Y731 and Y730 in RNR using different QM region sizes, as well as different functionals and basis sets. Specifically, we tested strings without the Y731-Y730 backbone or with two additional nearby residues, C439 and Q349, and showed that the mechanism remained unchanged with free energy barriers varying by less than ~2 kcal/mol. The computational expense of these simulations prevents the investigation of significantly larger QM regions. Based on the previous benchmarking, however, the qualitative results for PCET in RNR are expected to be captured with the QM regions used herein.

Starting from an MD equilibrated structure, we generated the initial guess of the reactant and product by placing the proton on either Y356:O or Y731:O (i.e., one of the two oxygen atoms), followed by 100 steps of energy minimization of the QM region atoms. We then generated an approximation of the transition state by moving the proton to the midpoint between Y356:O and Y731:O, followed by 200 steps of energy minimization of the QM region atoms with harmonic restraints using force constants of 200 kcal/mol $Å^{-2}$ on the reaction coordinates. All these energy minimizations were performed with the MM region atoms frozen. Subsequently, an initial string was generated using quadratic interpolation connecting the reaction coordinates associated with the QM region atoms for the reactant, approximated transition state, and product states. At least 20 images were evenly distributed along the string (Table S2), followed by 10 ps MD equilibration of the MM region with the QM region atoms fixed and 100 fs QM/MM MD equilibration of both the QM and the MM region atoms with 100 kcal/mol $Å^{-2}$ harmonic restraints on the reaction coordinates for each image.

After this initial equilibration, the iterative procedure for the QM/MM finite temperature string method with umbrella sampling was started. For each iteration, a new string was generated by quadratic interpolation over the average reaction coordinates for each image of the previous iteration, and a new set of images was redistributed evenly along this new string. Each image was associated with the values of the reaction coordinates determined from the quadratic interpolation. Each iteration entailed 100 fs of QM/MM MD sampling for each image with harmonic restraints applied to the reaction coordinates. The force constants for the harmonic restraints on the reaction coordinates were typically 100 kcal/mol $Å^{-2}$, although this value was increased to 200–400 kcal/mol $Å^{-2}$ for certain images that were more difficult to sample, such as the top of the barrier (Table S2).

We used the last iteration of the converged string to generate the minimum free energy path (MFEP). Data from all iterations was used to generate the multidimensional free energy surface using the free weighted histogram analysis method (WHAM).[26-27] The bin size was 0.1 Å and the convergence criterion was 0.001 for the WHAM procedure. A string was considered converged if the changes in the free energy barrier and reaction free energy was less than 0.1 kcal/mol for the last five iterations (Figure S4) with two exceptions. The mediated-stacked string, which is a water-mediated PCET mechanism with stacked Y731, has the largest QM region. Its free energy barrier and reaction free energy are extremely high, and therefore we used a convergence criterion of 1.0 kcal/mol to avoid expending computational effort on an unlikely mechanism. The direct-flipped-1 string, which is a direct PCET mechanism with flipped Y731, exhibited small oscillations on the order of < 1 kcal/mol in the reaction free energy and free energy barrier due to fluctuations of neighboring water molecules (Figure S6). In this case, we computed the MFEP from the iteration corresponding to the lowest free energy barrier and reaction free energy. We also note that the original string for this case did not sufficiently sample the Y731$^{\bullet}$ region and excessively sampled the Y356$^{\bullet}$. Thus, after removing the first three images on the Y356$^{\bullet}$ end, extrapolating four images on the Y731$^{\bullet}$ end, and redistributing all the images evenly along the string, we started a new string that sufficiently sampled both the reactant and the product states. For consistency, the free energy surface reported for this string only includes data from the new string, which was started from an iteration labeled 1 and propagated for a total of 60 iterations. Bootstrapping[26, 28] was performed by generating 100 bootstrapped free energy profiles, and the standard deviations of these free energy profiles are given as error bars in Figure S5. Note that bootstrapping provides only statistical errors and does not account for uncertainties due to the level of theory and computational methods.

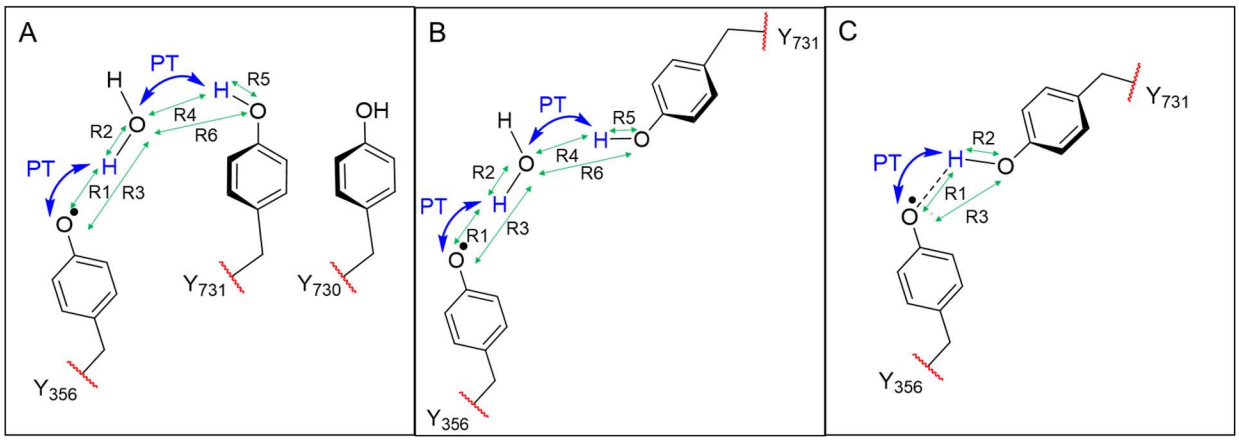

Figure S1. QM region and reaction coordinates used in the QM/MM string simulations for (A) water-mediated PCET mechanism with stacked Y731, (B) water-mediated PCET mechanism with flipped Y731, and (C) direct PCET mechanism with flipped Y731. The strings simulating the water-mediated PCET mechanism used six reactions: the distance between the hydroxyl oxygen of Y356 and the oxygen of the bridging water, the distance between the transferring hydrogen and each of these oxygens, the distance between the oxygen of Y731 and the bridging water, and the distance between the transferring hydrogen from Y731 and each of these oxygens. The red dashes indicate the placement of link atoms. The strings simulating the direct PCET mechanism used three reaction coordinates: the distance between the hydroxyl oxygens of Y356 and Y731 and the distance between the transferring hydrogen and each of these oxygens.

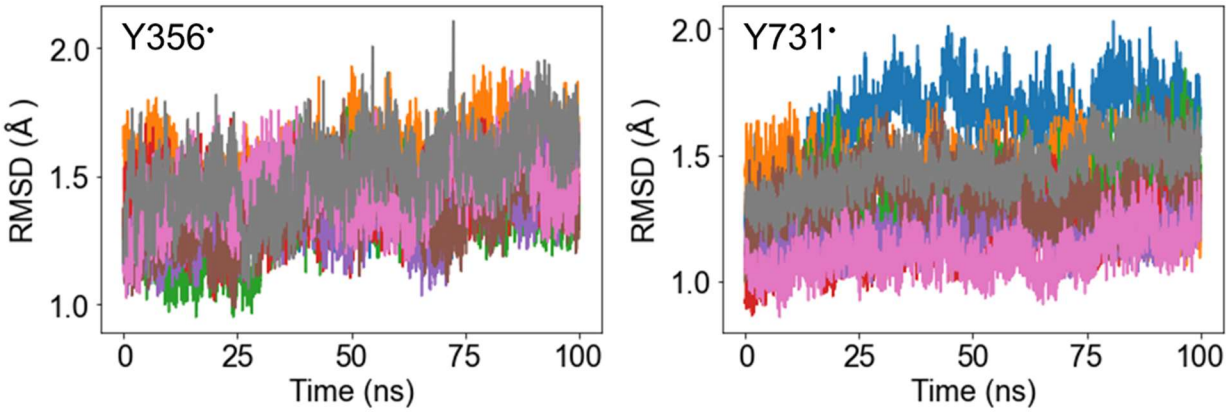

Figure S2. RMSD for the C_α atoms in the α/β subunits over all production trajectories with respect to the cryo-EM structure. The average RMSD was 1.42 ± 0.15 Å for the system with Y356• and 1.33 ± 0.19 Å for the system with Y731•. The different colors correspond to the eight independent 100 ns trajectories for each system. The RMSD increased to ~2.23 Å and ~1.85 Å when C_α atoms from the α′/β′ subunits are included as well.

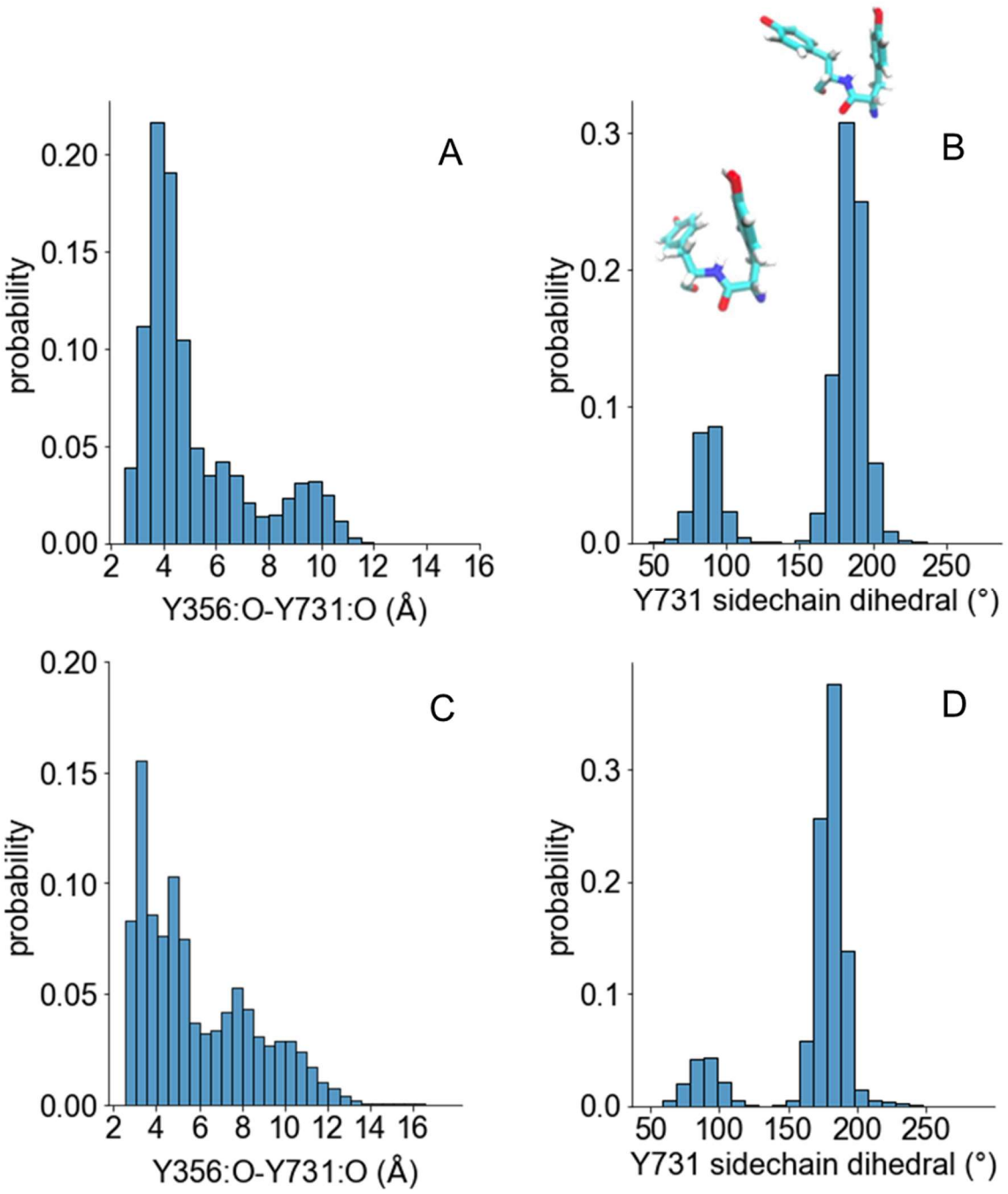

Figure S3. Distribution of distance between oxygen atoms of Y356 and Y731 and distribution of the N-C_α-C_β-C_γ dihedral angle χ in the Y731 sidechain obtained from the (A,B) Y356$^\bullet$ and (C,D) Y731$^\bullet$ classical MD simulations. The bin size is 0.5 Å for the distance and 10˚ for the angle. Each distribution was obtained over 8 × 100 ns independent classical MD trajectories. The average distance between the oxygen atoms of Y356 and Y731 was 5.1 ± 2.1 Å for the Y356$^\bullet$ simulations and 5.9 ± 2.6 Å for the Y731$^\bullet$ simulations. For most conformations sampled, Y731 was flipped out toward the α/β interface ($\chi \approx 182.5^o$), and for a small number of conformations, Y731 was in what was previously denoted the off-pathway orientation ($\chi \approx 77.5^o$).

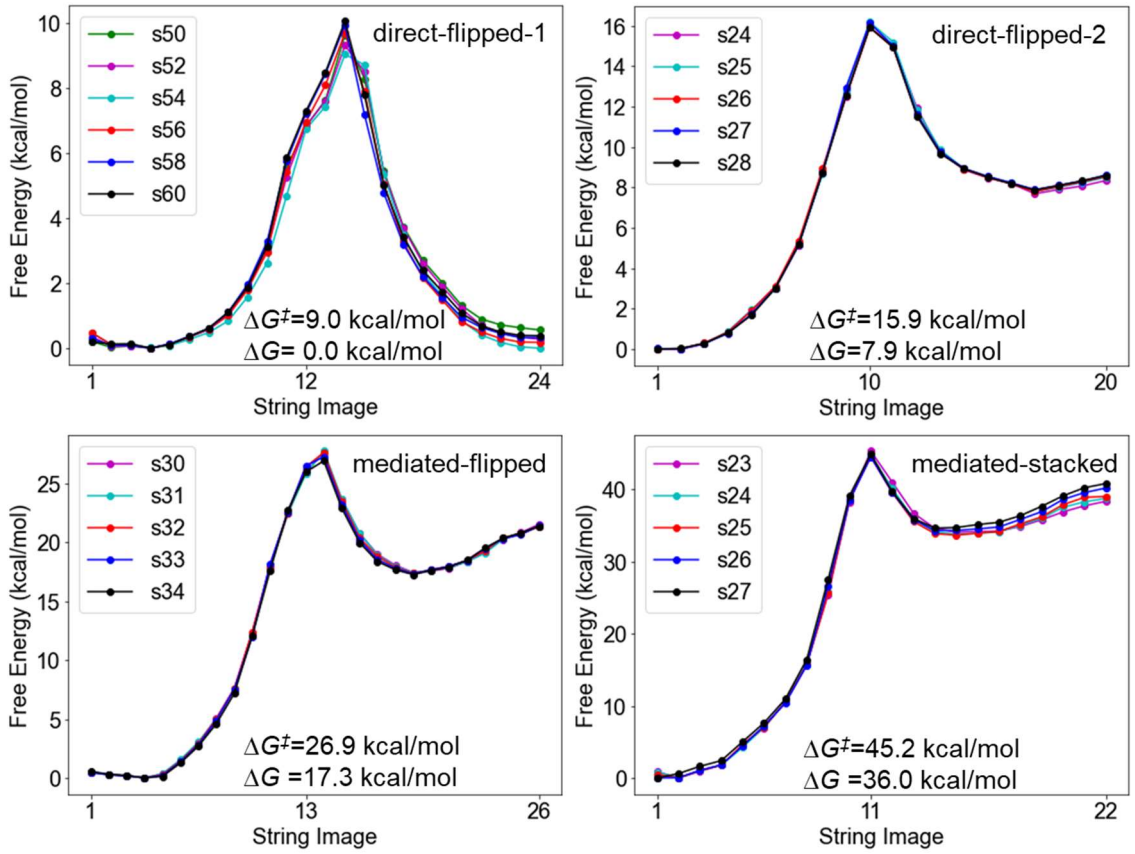

Figure S4. Free energy profiles along the MFEPs for the four strings simulated. Free energy profiles for every two iterations from iteration 50 to 60 (direct-flipped-1) or for the last five iterations (direct-flipped-2, mediated-flipped, mediated-stacked) are shown. Further details of the direct-flipped-1 string's small oscillations are provided in Figure S6. The converged free energy barriers and reaction free energies for radical transfer from Y356 to Y731 are given at the bottom of each panel, as also given in Table 1 of the main paper.

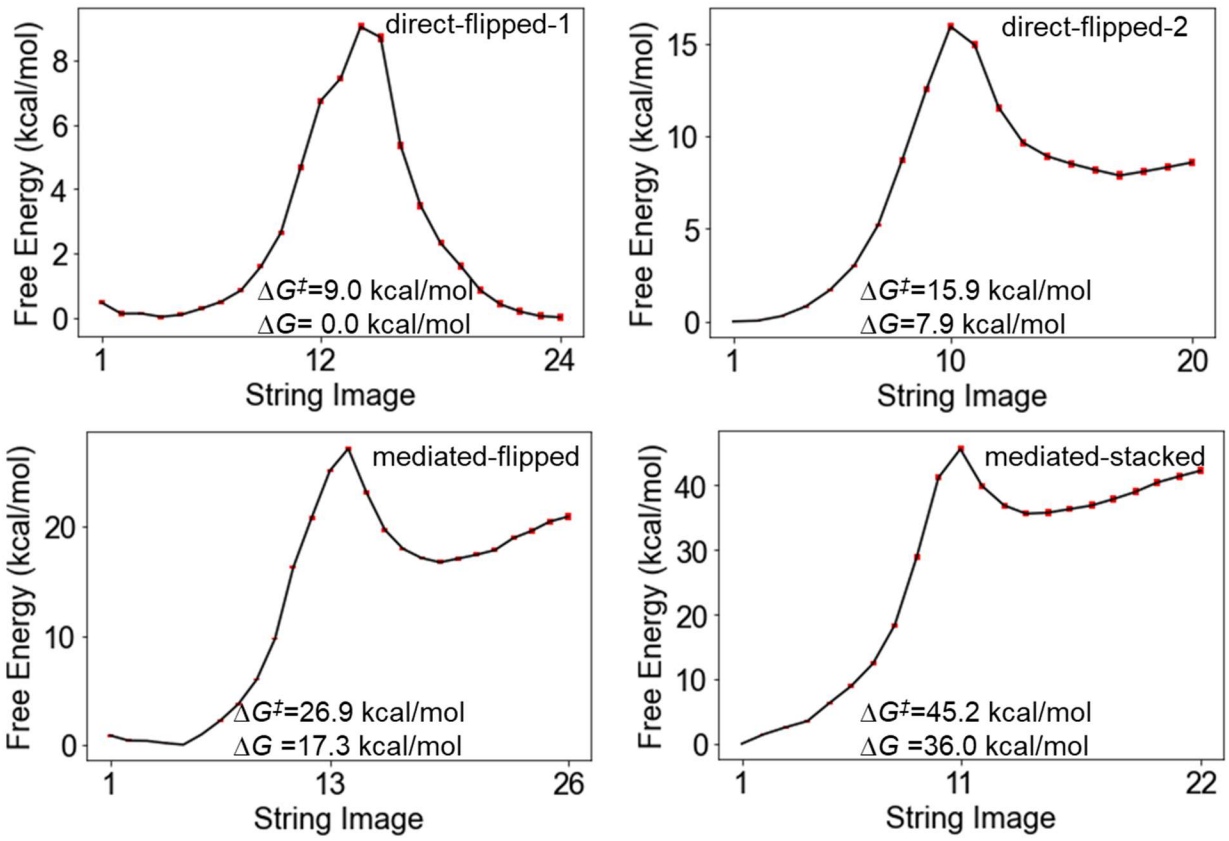

Figure S5. Free energy profiles along the MFEPs for iteration 54 of the direct-flipped-1 string and for the last iteration of the other three strings including error bars from bootstrapping shown in red. Note that bootstrapping provides only statistical errors and does not account for uncertainties due to the level of theory and computational methods.

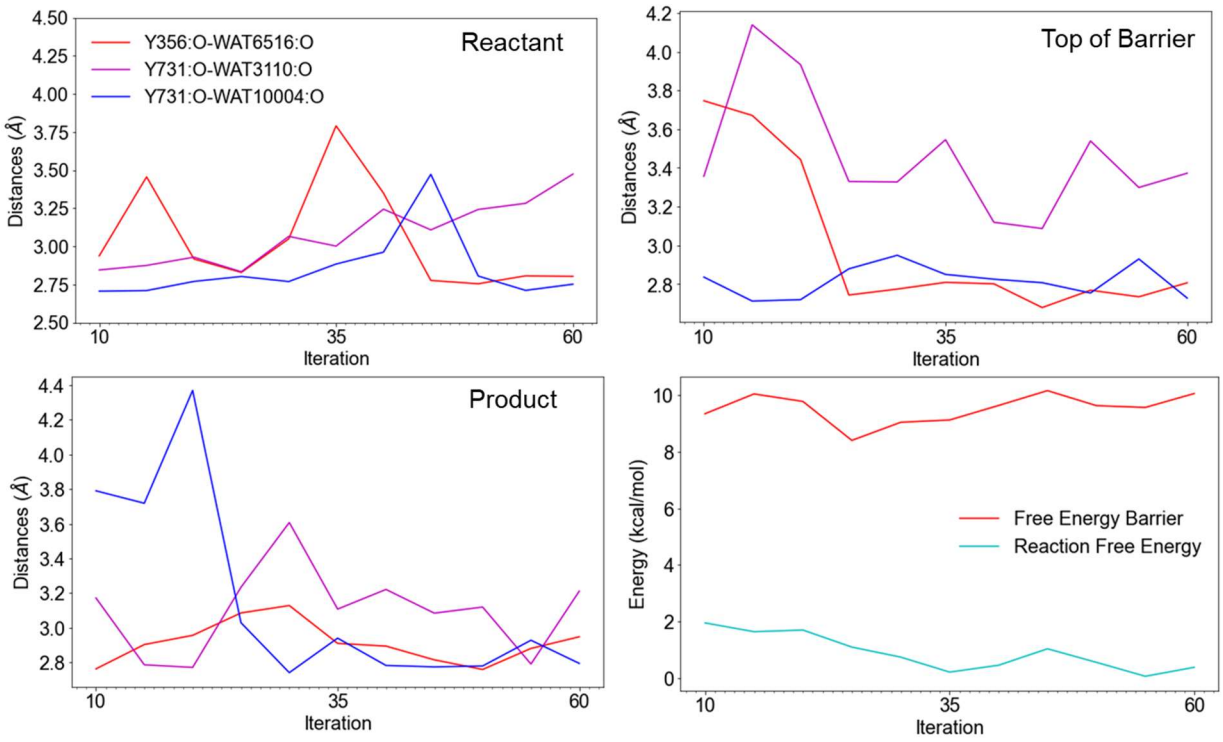

Figure S6. Analysis of the free energy barrier and reaction free energy, as well as interactions with water molecules, for the direct-flipped-1 string. The lower right panel shows the free energy barrier and reaction free energy as a function of iteration, illustrating the small oscillations that appear due to motions of the neighboring water molecules. The other panels show the average distances between the oxygen atoms of Y356 or Y731 and water molecules within ~3 Å for the images corresponding to the reactant, top of the barrier, and product. Data is shown for every five iterations from iteration 10 to 60.

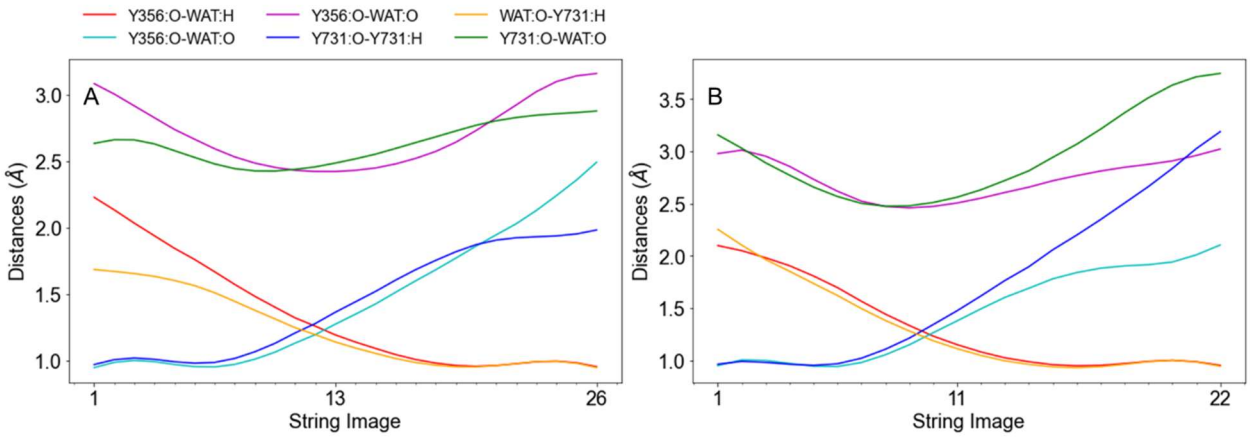

Figure S7. Reaction coordinates for the water-mediated PCET strings with (A) Y731 in the flipped conformation and (B) Y731 in the stacked conformation. Both water-mediated mechanisms show concerted double proton transfer between Y356 and water and between Y731 and water.

Table S1. Comparison of Average Distances[a] for Strings Simulating Water-Mediated Radical Transfer from Y356 to Y731.

	Y356O–WATH	WATO–WATH	Y356O–WATO	Y731O–Y731H	WATO–Y731H	Y731O-WATO
mediated-flipped						
Reactant	1.84	0.97	2.74	0.99	1.60	2.58
Top of barrier	1.14	1.35	2.43	1.44	1.09	2.52
Product	0.96	1.77	2.64	1.82	0.95	2.73
mediated-stacked						
Reactant	2.10	0.95	2.98	0.96	2.25	3.16
Top of barrier	1.15	1.38	2.51	1.48	1.11	2.56
Product	0.99	1.69	2.66	1.90	0.96	2.81

[a] The distances in Angstroms between the transferring hydrogen and each of the tyrosine/water oxygens (denoted Y356O–WATH, Y731O–Y731H, WATO-WATH, and WATO-Y731H) and between the oxygens of Y356/Y731 and water (denoted Y356O–WATO and Y731O-WATO) were averaged over the final iteration for the images closest to the reactant, top of the barrier, and product for the two strings.

Table S2. Images with More than 100 kcal/mol Å^{-2} Harmonic Restraints on Reaction Coordinates during QM/MM String Simulations of Radical Transfer from Y356 to Y731.

String	Restraints (kcal/mol Å^{-2})	Reaction Coordinates	Iterations	Images
direct-flipped-1	200	R1, R2	0	10-14
			1-4	11-13
			5-9	2, 12-13
			10	11-12
			17-28	12-13
	300	R1-R3	0	20-24
			1,2,11,12,14	1
			3-9	1,10
			10	10
	400	R1-R2	11-15, 29-62	11-13
			17-28	11
direct-flipped-2	200	R1-R3	0-1	1-22
		R1-R2	2-3	1-11,13-22
			4	1,2,10-14
			5-13	1,2,9,10,12-14
			14	1,11
			15	1,9-12
			16-17	1,11
			18	11
		R3	2-3	1-12
	300	R1-R2	2-3	10-12
			5-7,9,10	11
mediated-flipped	200	R1-R6	0, 7-9,11-19	1-26
			1-6	1-21
		R3, R6	1-6	22-28
	300	R1-R2, R4-R5	1-6	22-28
			20-38	14
mediated-stacked	200	R1-R6	0-1,10-15	1-22
		R1-R2, R4-R5	17-21	10-13
	300	R1-R2, R4-R5	2-9	1-22
	300	R1-R6	10	12

References

(1) Reinhardt, C. R.; Li, P.; Kang, G.; Stubbe, J.; Drennan, C. L.; Hammes-Schiffer, S., Conformational Motions and Water Networks at the α/β Interface in E. coli Ribonucleotide Reductase. *J. Am. Chem. Soc.* **2020,** *142*, 13768-13778.
(2) Reinhardt, C. R.; Sayfutyarova, E. R.; Zhong, J.; S., H.-S., Glutamate Mediates Proton-Coupled Electron Transfer Between Tyrosines 730 and 731 in Escherichia coli Ribonucleotide Reductase. *J. Am. Chem. Soc.* **2021,** *143*, 6054-6059.
(3) Zhong, J.; Reinhardt, C. R.; Hammes-Schiffer, S., Role of Water in Proton-Coupled Electron Transfer between Tyrosine and Cysteine in Ribonucleotide Reductase. *J. Am. Chem. Soc.* **2022,** *144*, 7208–7214.
(4) Kang, G.; Taguchi, A. T.; Stubbe, J.; Drennan, C. L., Structure of a trapped radical transfer pathway within a ribonucleotide reductase holocomplex. *Science* **2020,** *368*, 424-427.
(5) Gordon, J. C.; Myers, J. B.; Folta, T.; Shoja, V.; Heath, L. S.; Onufriev, A., H++: a server for estimating pKas and adding missing hydrogens to macromolecules *Nucleic Acids Res.* **2005,** *33*, W368-W371.
(6) Jorgensen, W. L. C., J.; Madura, J. D.; Impey, R. W.; Klein, M. L. , Comparison of simple potential functions for simulating liquid water. *J. Chem. Phys.* **1983,** *79*, 926-935.
(7) Maier, J. A.; Martinez, C.; Kasavajhala, K.; Wickstrom, L.; Hauser, K. E.; Simmerling, C., ff14SB: Improving the Accuracy of Protein Side Chain and Backbone Parameters from ff99SB. *J. Chem. Theory Comput.* **2015,** *11*, 3696-3713.
(8) Li, P.; Merz Jr, K. M., MCPB.py: A Python Based Metal Center Parameter Builder. *J. Chem. Inf. Model.* **2016,** *56*, 599-604.
(9) Bayly, C. I. C., P.; Cornell, W.; Kollman, P. A A well-behaved electrostatic potential based method using charge restraints for deriving atomic charges: the RESP model. *J. Phys. Chem. Lett.* **1993,** *97*, 10269-10280.
(10) Darden, T.; York, D.; Pedersen, L., Particle mesh Ewald: An N·log(N) method for Ewald sums in large systems. *J. Chem. Phys.* **1993,** *98*, 10089-10092.
(11) Ryckaert, J.-P.; Ciccotti, G.; Berendsen, H. J., Numerical integration of the cartesian equations of motion of a system with constraints: molecular dynamics of n-alkanes. *J. Comp. Phys.* **1977,** *23*, 327-341.
(12) Miyamoto, S.; Kollman, P. A., SETTLE: an analytical version of the SHAKE and RATTLE algorithm for rigid water models. *J. Comput. Chem.* **1992,** *13*, 952-962.
(13) Michaud-Agrawal, N.; Denning, E. J.; Woolf, T. B.; Beckstein, O., MDAnalysis: A Toolkit for the Analysis of Molecular Dynamics Simulations. *J. Comput. Chem.* **2011,** *32*, 2319-2327.
(14) Gowers, R. J.; Linke, M.; Barnoud, J.; Reddy, T. J. E.; Melo, M. N.; Seyler, S. L.; Dotson, D. L.; Domanski, J.; Buchoux, S.; Kenney, I. M.; Beckstein, O., MDAnalysis: A Python package for the rapid analysis of molecular dynamics simulations. In *Proceedings of the 15th Python in Science Conference*, Benthall, S.; Rostrup, S., Eds. Austin, TX, 2016; pp 98-105.
(15) Case, D. A.; Cheatham, T. E.; Darden, T.; Gohlke, H.; Luo, R.; Merz, K. M.; Onufriev, A.; Simmerling, C.; Wang, B.; Woods, R. J., The Amber biomolecular simulation programs. *J. Comput. Chem.* **2005,** *26*, 1668-1688.
(16) Gotz, A. W.; Clark, M. A.; Walker, R. C., An extensible interface for QM/MM molecular dynamics simulations with AMBER. *J. Comput. Chem.* **2014,** *35*, 95-108.
(17) Shao, Y.; Gan, Z.; Epifanovsky, E.; Gilbert, A. T.; Wormit, M.; Kussmann, J.; Lange, A. W.; Behn, A.; Deng, J.; Feng, X.; Ghosh, D.; Goldey, M. B.; Horn, P. R.; Jacobson, L.; Kaliman, I.; Khaliullin, R. Z.; Kus, T.; Landau, A.; Liu, J.; Proynov, E. I.; Rhee, Y. M.; Richard, R. M.;

Rohrdanz, M. A.; Steele, R. P.; Sundstrom, E.; Woodcock, H. L.; Zimmerman, P. M.; Zuev, D.; Albrecht, B. J.; Alguire, E. C.; Austin, B.; Beran, G. J.; Bernard, Y. A.; Berquist, E. J.; Brandhorst, K.; Bravaya, K. B.; Brown, S. T.; Casanova, D.; Chang, C.; Chen, Y.; Chien, S.; Closser, K. D.; Crittenden, D. L.; Diedenhofen, M.; Distasio, R. A.; Do, H.; Dutoi, A. D.; Edgar, R. G.; Fatehi, S.; Fusti-Molnar, L.; Ghysels, A.; Golubeva-Zadorozhnaya, A.; Gomes, J.; Hanson-Heine, M. W.; Harbach, P. H.; Hauser, A. W.; Hohenstein, E. G.; Holden, Z. C.; Jagau, T.; Ji, H.; Kaduk, B. J.; Khistyaev, K.; Kim, J.; Kim, J.; King, R. A.; Klunzinger, P. E.; Kosenkov, D.; Kowalczyk, T.; Krauter, C. M.; Lao, K. U.; Laurent, A. D.; Lawler, K. V.; Levchenko, S. V.; Lin, C. Y.; Liu, F.; Livshits, E.; Lochan, R. C.; Luenser, A.; Manohar, P.; Manzer, S. F.; Mao, S.; Mardirossian, N.; Marenich, A. V.; Maurer, S. A.; Mayhall, N. J.; Neuscamman, E.; Oana, C. M.; Olivares-Amaya, R.; O'Neill, D. P.; Parkhill, J. A.; Perrine, T. M.; Peverati, R.; Prociuk, A.; Rehn, D. R.; Rosta, E.; Russ, N. J.; Sharada, S. M.; Sharma, S.; Small, D. W.; Sodt, A. J.; Stein, T.; Stück, D.; Su, Y.; Thom, A. J.; Tsuchimochi, T.; Vanovschi, V.; Vogt, L.; Vydrov, O. A.; Wang, T.; Watson, M.; Wenzel, J.; White, A. F.; Williams, C. F.; Yang, J.; Yeganeh, S.; Yost, S.; You, Z.; Zhang, I. Y.; Zhang, X.; Zhao, Y.; Brooks, B. R.; Chan, G. K.; Chipman, D. M.; Cramer, C. J.; Goddard, W. A.; Gordon, M. S.; Hehre, W. J.; Klamt, A.; Schaefer, H. F.; Schmidt, M. W.; Sherrill, C. D.; Truhlar, D. G.; Warshel, A.; Xu, X.; Aspuru-Guzik, A.; Baer, R.; Bell, A. T.; Besley, N. A.; Chai, J.; Dreuw, A.; Dunietz, B. D.; Furlani, T. R.; Gwaltney, S. R.; Hsu, C.; Jung, Y.; Kong, J.; Lambrecht, D. S.; Liang, W.; Ochsenfeld, C.; Rassolov, V. A.; Slipchenko, L. V.; Subotnik, J. E.; Van Voorhis, T.; Herbert, J. M.; Krylov, A. I.; Gill, P. M.; Head-Gordon, M., Advances in molecular quantum chemistry contained in the Q-Chem 4 program package. *Molecular Physics* **2015,** *113*, 184-215.

(18) Chai, J.-D.; Head-Gordon, M., Long-range corrected hybrid density functionals with damped atom–atom dispersion corrections. *Phys. Chem. Chem. Phys.* **2008,** *10*, 6615-6620.

(19) Hehre, W. J.; Ditchfield, R.; Pople, J. A., Self-consistent molecular orbital methods. XII. Further extensions of Gaussian—type basis sets for use in molecular orbital studies of organic molecules. *J. Chem. Phys.* **1972,** *56*, 2257-2261.

(20) Harihara.Pc; Pople, J. A., Influence of Polarization Functions on Molecular-Orbital Hydrogenation Energies. *Theor. Chim. Acta.* **1973,** *28*, 213-222.

(21) Clark, T.; Chandrasekhar, J.; Spitznagel, G. W.; Schleyer, P. V. R., Efficient diffuse function-augmented basis sets for anion calculations. III. The 3-21+G basis set for first-row elements, Li–F. *J. Comput. Chem.* **1983,** *4*, 294-301.

(22) Cornell, W. D.; Cieplak, P.; Bayly, C. I.; Gould, I. R.; Merz, K. M.; Ferguson, D. M.; Spellmeyer, D. C.; Fox, T.; Caldwell, J. W.; Kollman, P. A., A Second Generation Force Field for the Simulation of Proteins, Nucleic Acids, and Organic Molecules. *J. Am. Chem. Soc.* **1995,** *117*, 5179-5197.

(23) Cheatham, T. E.; Cieplak, P.; Kollman, P. A., A Modified Version of the Cornell et al. Force Field with Improved Sugar Pucker Phases and Helical Repeat. *J. Biomol. Struct. Dyn.* **1999,** *16*, 845-862.

(24) Hornak, V.; Abel, R.; Okur, A.; Strockbine, B.; Roitberg, A.; Simmerling, C., Comparison of multiple Amber force fields and development of improved protein backbone parameters. *Proteins* **2006,** *65*, 712-725.

(25) Kulik, H. J., Large-scale QM/MM free energy simulations of enzyme catalysis reveal the influence of charge transfer. *Phys. Chem. Chem. Phys.* **2018,** *20*, 20650-20660.

(26) Grossfield, A. *WHAM: the weighted histogram analysis method.*, WHAM version 2.0.9.

(27) Souaille, M.; Roux, B. t., Extension to the weighted histogram analysis method: combining umbrella sampling with free energy calculations. *Comput. Phys. Commun.* **2001,** *135*, 40-57.

(28) Hub, J. S.; de Groot, B. L.; van der Spoel, D., g_wham—A Free Weighted Histogram Analysis Implementation Including Robust Error and Autocorrelation Estimates. *J. Chem. Theory Comput.* **2010,** *6*, 3713-3720.